Int. J. Heat Mass Transfer. Vol. 20, pp. 269–277. Pergamon Press 1977. Printed in Great Britain

STABLE FILM BOILING HEAT TRANSFER FROM FLAT HORIZONTAL PLATES FACING DOWNWARDS

M. M. FARAHAT
Argonne National Laboratory, Argonne, IL 60439, U.S.A.

and

E. E. MADBOULY
Graduate Student, Department of Nuclear Engineering, University of Alexandria, Egypt

(*Received* 26 *November* 1975 *and in revised form* 9 *April* 1976)

Abstract—An analysis is presented for stable, laminar, free-convection, film-boiling heat-transfer from an isothermal, horizontal, flat circular plate facing downward and submerged in a saturated liquid.

The mathematical techniques of boundary-layer theory are used, and the continuity, momentum, and energy equations for the vapour phase are solved numerically using an explicit difference technique.

Results are obtained for saturated water at atmospheric pressure and at plate temperatures at 450–1050°C and plate diameters up to 250 mm.

NOMENCLATURE

- c_p, specific heat at constant pressure;
- D, diameter;
- Gr, Grashof number;
- g, gravitational acceleration;
- H, reference length;
- h, heat-transfer coefficient;
- k, thermal conductivity;
- Nu, Nusselt number;
- Pr, Prandtl number;
- q'', heat flux;
- R, dimensionless radial coordinate;
- R_0, dimensionless plate radius;
- r, radial coordinate;
- r_0, plate radius;
- T, temperature;
- ΔT_s, wall superheat, $T_w - T_s$;
- t, time;
- U, dimensionless velocity component in the x-direction;
- u, velocity component in the x-direction;
- V, dimensionless radial velocity component;
- v, radial velocity component;
- X, dimensionless axial coordinate;
- x, axial coordinate.

Greek symbols

- α, thermal diffusivity;
- β, coefficient of volume expansion of vapour;
- δ, vapour film thickness;
- λ, latent heat of vaporization;
- λ^*, modified latent heat of vaporization, $\lambda + c_p \Delta T_s/2$.
- θ, dimensionless temperature;
- μ, viscosity;
- ρ, density;
- τ, dimensionless time.

Subscripts

- l, liquid;
- s, saturation;
- w, wall;
- δ, interface.

Superscripts

- $'$, after a time step $\Delta\tau$;
- $\bar{}$, average value.

1. INTRODUCTION

SINCE Bromley's pioneering work in film boiling was published in 1948 [1], many studies were conducted in that area. Geometry of the heating surface was a key variable in these investigations. This ranged from horizontal wires, tubes, and flat plates; to vertical cylinders and plates; to spheres and hemispheres.

One of the few geometries that remains practically uninvestigated is the flat horizontal plate facing downwards. It is the purpose of the present work to analyse stable film boiling heat transfer from downward facing flat horizontal plated, when placed in a saturated liquid.

Chang [2] presented a wave theory of film boiling heat transfer. He suggested that a certain similarity existed between small, vertical and downfacing, plates. Bromley [3] showed that for vertical plates, the Nusselt number for film boiling is given by

$$Nu = 0.62[(Gr \cdot Pr)(0.4 + \lambda/c_p \Delta T_s)]^{1/4}. \quad (1)$$

Ishigai *et al.* [4] conducted an experimental study of pool boiling from downward facing plates of different diameters to saturated water. They noticed that burnout occurred at a much lower heat flux than that for plates facing upward. As the plate diameter increased the heat flux dropped appreciably in all regions of the boiling curve.

Githingi and Sabersky [5] investigated the effect of orientation of the heating surface on pool boiling of isopropyl alcohol up to burnout. They concluded that the heat flux at the burnout point for the plate facing downward is several times lower than that facing upward.

Anderson and Bova [6], studied the effects of plate diameter and wall superheat on pool boiling of Freon-11 up to burnout. They concluded that as the plate diameter increased (up to one foot), the average burnout heat flux decreased.

2. ANALYSIS

It is assumed in the present analysis that the vapour film forms under the plate surface and flows from the center towards the plate edge and up around the periphery where it is discharged. No effort is made to include the effect of vapour discharge on the flow pattern near the edge. The flow induces a horizontal movement in the liquid at the liquid-vapour interface due to the viscous friction encountered between the two phases.

Basic model and assumptions

Consider a horizontal circular plate at a uniform lower surface temperature T_w, Fig. 1, immersed in a saturated liquid at T_s. The plate surface temperature is higher than the Leidenfrost temperature of the liquid, enough to sustain stable film boiling.

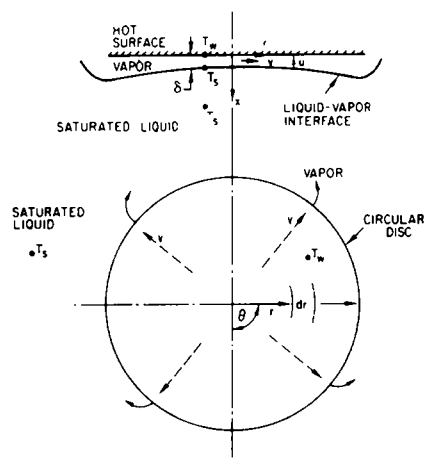

FIG. 1. Proposed model for film boiling from a downward facing circular plate.

Heat is transferred from the plate to the liquid-vapour interface by conduction, convection, and radiation through the vapour film. All the energy leaving the plate surface reaches the interface and is used totally to form vapour. The vapour flows radially toward the edge of the plate in the form of a thin vapour film and is eventually released.

The following assumptions are made,

1. The vapour film is thin and the flow of vapour beneath the plate is laminar and incompressible.
2. End effects are not considered.
3. The thin vapour film is treated as a laminar boundary layer.

Governing equations

The time dependent continuity, momentum, and energy equations in the x-direction are given in cylindrical coordinates with the following simplifications,

1. There is complete symmetry in the θ-direction.
2. $\partial^2 u/\partial x^2$ and $g(\rho_s - \bar{\rho})$ are neglected in comparison with other terms of the momentum equation.

Continuity

$$\frac{\partial v}{\partial r} + \frac{v}{r} + \frac{\partial u}{\partial x} = 0 \tag{2}$$

Momentum

$$\rho\left(\frac{\partial u}{\partial t} + v\frac{\partial u}{\partial r} + u\frac{\partial u}{\partial x}\right) = -\beta\rho_s g(T - T_s) + \mu\left(\frac{\partial^2 u}{\partial r^2} + \frac{1}{r}\frac{\partial u}{\partial r}\right) \tag{3}$$

Energy

$$\rho c_p\left[\frac{\partial T}{\partial t} + v\frac{\partial T}{\partial r} + u\frac{\partial T}{\partial x}\right] = k\left[\frac{1}{r}\frac{\partial}{\partial r}\left(r\frac{\partial T}{\partial r}\right) + \frac{\partial^2 T}{\partial x^2}\right]. \tag{4}$$

Although the primary goal is to obtain the steady state solution of the problem for which $\partial u/\partial t$ and $\partial T/\partial t$ are both zero, one way such a solution may be achieved is by considering the unsteady state problem already formulated above. Successive steps in time may then be regarded as successive approximations toward the final steady state solution. The initial and boundary conditions are,

$$\text{for } t = 0: \quad u = v = 0, \quad T = T_s \tag{5}$$

$$\text{for } t > 0: \text{ at } r = 0, \quad v = 0$$

$$\text{at } x = 0, \ u = v = 0, \quad T = T_w \tag{6}$$

$$\text{at } x = \delta, \ -k\left.\frac{\partial T}{\partial x}\right|_{x=0} = \rho\lambda^* u_\delta, \ T = T_s.$$

We have a system of partial differential equations and associated boundary conditions. These are solved by an explicit difference method [7].

Dimensionless equations

The following dimensionless forms of temperature, space coordinates, velocity, and time are used,

$$\theta = \frac{T - T_s}{T_w - T_s} \tag{7}$$

$$R = \frac{r}{H} \tag{8}$$

$$X = \left(\frac{B}{\mu\alpha H}\right)^{\frac{1}{4}} \cdot x \tag{9}$$

$$U = \left(\frac{\mu H}{\alpha^3 B}\right)^{\frac{1}{4}} \cdot u \tag{10}$$

$$V = \left(\frac{\mu}{B\alpha H}\right)^{\frac{1}{4}} \cdot v \tag{11}$$

$$\tau = \left(\frac{\alpha B}{\mu H}\right)^{\frac{1}{2}} \cdot t \tag{12}$$

where: B = constant $[-g\rho_s(T - T_s)\beta]$, and H = arbitrary reference length.

Substituting equations (7)–(12) into equations (2)–(4), we get the following system of dimensionless partial differential equations,

$$\frac{\partial U}{\partial X}+\frac{\partial V}{\partial R}+\frac{V}{R}=0 \tag{13}$$

$$\frac{\partial U}{\partial \tau}+U\frac{\partial U}{\partial X}+V\frac{\partial U}{\partial R}=C_4\left(\frac{\partial^2 U}{\partial R^2}+\frac{1}{R}\frac{\partial U}{\partial R}+C\theta\right) \tag{14}$$

$$\frac{\partial \theta}{\partial \tau}+U\frac{\partial \theta}{\partial X}+V\frac{\partial \theta}{\partial R}=\frac{\partial^2 \theta}{\partial X^2}+\frac{C_1}{R}\frac{\partial \theta}{\partial R} \tag{15}$$

where:
$$C=\frac{H^2 B}{\mu}\left(\frac{\mu H}{\alpha^3 B}\right)^{\frac{1}{4}} \tag{16}$$

$$C_1=\left(\frac{\mu\alpha}{BH^3}\right)^{\frac{1}{4}} \tag{17}$$

$$C_4=\frac{\mu}{\rho H^2}\left(\frac{\mu H}{\alpha B}\right)^{\frac{1}{4}}. \tag{18}$$

Initial and boundary conditions,

for $\tau=0$, $U=V=\theta=0$ (19)

for $\tau>0$, at $R=0$, $V=0$

at $X=0$, $U=V=0$, $\theta=1$ (20)

at the interface,

$$-C_5\left.\frac{\partial \theta}{\partial X}\right|_{x=0}=U_\delta,\ \theta=0 \tag{21}$$

where: $C_5=\dfrac{k(T_w-T_s)}{\rho\lambda^*\alpha}$.

Numerical solution

The space of investigation is divided into m and n grid spacings in the X and R directions respectively as shown in Figs. 2(a, b). Let F' denote the value of the variable F at the end of a time step $\Delta\tau$, as shown in Fig. 3. An appropriate set of finite difference equations corresponding to equations (13)–(15) is,

$$\frac{V(i,j)-V(i,j-1)}{\Delta R}+\frac{U(i+1,j)-U(i,j)}{\Delta X}+\frac{V(i,j)}{R(j)}=0 \tag{22}$$

$$\frac{U'(i,j)-U(i,j)}{\Delta\tau}+U(i,j)\frac{U(i+1,j)-U(i,j)}{\Delta X}+V(i,j)\frac{U(i,j)-U(i,j-1)}{\Delta R}=C_4\frac{U(i,j+1)-2U(i,j)+U(i,j-1)}{(\Delta R)^2}-\frac{C_4}{R(j)}\frac{U(i,j)-U(i,j-1)}{\Delta R}+CC_4\theta'(i,j) \tag{23}$$

$$\frac{\theta'(i,j)-\theta(i,j)}{\Delta\tau}+U(i,j)\frac{\theta(i+1,j)-\theta(i,j)}{\Delta X}+V(i,j)\frac{\theta(i,j)-\theta(i,j-1)}{\Delta R}=\frac{\theta(i+1,j)-2\theta(i,j)+\theta(i-1,j)}{(\Delta X)^2}-\frac{C_1}{R(j)}\frac{\theta(i,j)-\theta(i,j-1)}{\Delta R}. \tag{24}$$

During any one time step $\Delta\tau$ the coefficients $U(i,j)$, $V(i,j)$, and $R(j)$ are treated as constants. At the end of any time step the new temperatures and velocity components θ', U', V' at all interior grid points may be obtained by successive application of equations (24), (23), (22) respectively. This process is repeated, and provided the time step is sufficiently small, U, V, θ should eventually converge to values which approximate the steady state solution of equations (13)–(15).

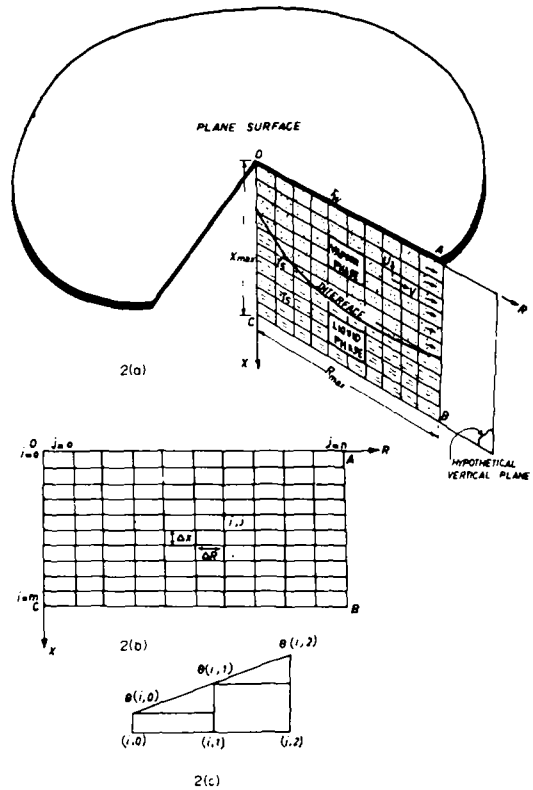

FIG. 2(a). Vertical cross section in the plate, vapour film, and saturated liquid.
FIG. 2(b). The space grid.
FIG. 2(c). Linear temperature distribution near the plate axis.

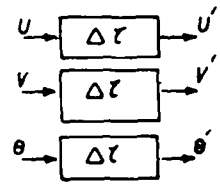

FIG. 3. Time-step block diagram.

Temperature distribution along the plate axis

Since the vapour film thickness beneath the plate centre is not zero, an approximation is introduced to evaluate the temperature along the axis. The temperature distribution in the radial direction is assumed linear between the axis and the two nodal points in the same horizontal level next to the axis, Fig. 2(c), thus, $\theta(i,0)=2\theta(i,1)-\theta(i,2)$.

Determination of the liquid–vapour interface

The position of the interface can be located by satisfying the boundary conditions at the interface which are,

$$-C_5\left.\frac{\partial \theta}{\partial X}\right|_{x=0}=U_\delta,\quad \theta=0.$$

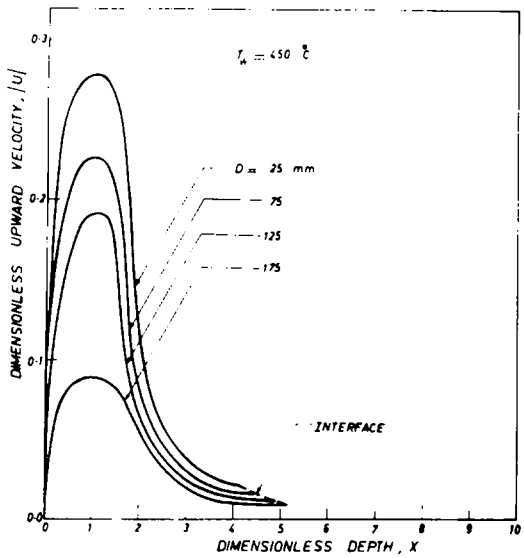

FIG. 4(a). Variation of upward velocity component with depth, $T_w = 450°C$.

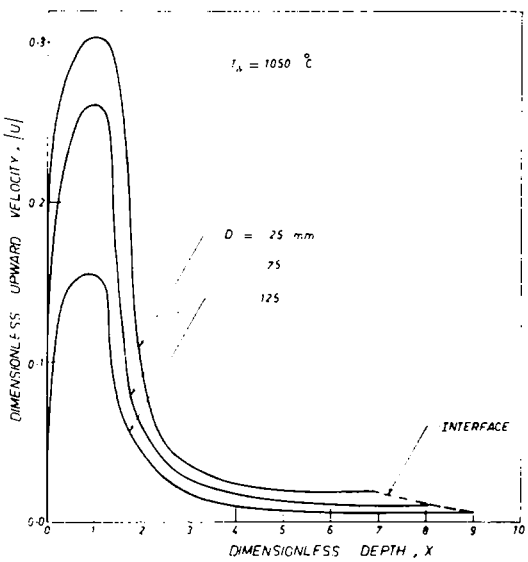

FIG. 4(b). Variation of upward velocity component with depth, $T_w = 1050°C$.

Local heat flux and heat-transfer coefficient

$$q''(r) = -k\left.\frac{\partial T}{\partial x}\right|_{x=0}$$

hence,

$$q''(R) = -k\Delta T_s\left(\frac{B}{\mu\alpha\overline{H}}\right)^{\frac{1}{4}}\cdot\left.\frac{\partial\theta}{\partial\overline{X}}\right|_{X=0} \quad (25)$$

$$h(R) = q''(R)/\Delta T_s = -k\left(\frac{B}{\partial\alpha\overline{H}}\right)^{\frac{1}{4}}\cdot\left.\frac{\partial\theta}{\partial\overline{X}}\right|_{X=0}. \quad (26)$$

Average heat flux and heat-transfer coefficient

$$\overline{q''(R_0)} = \frac{1}{R_0}\int_0^{R_0} q''(R)\,dR \quad (27)$$

$$\bar{h}(\bar{R}_0) = \frac{1}{R_0}\int_0^{R_0} h(R)\,dR. \quad (28)$$

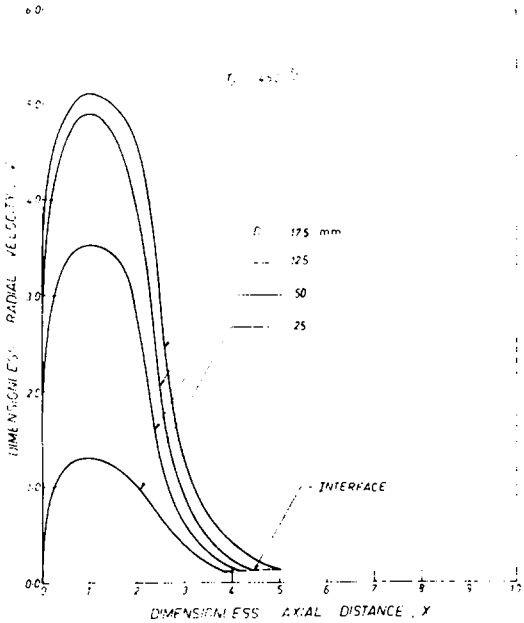

FIG. 5(a). Variation of radial velocity with depth, $T_w = 450°C$.

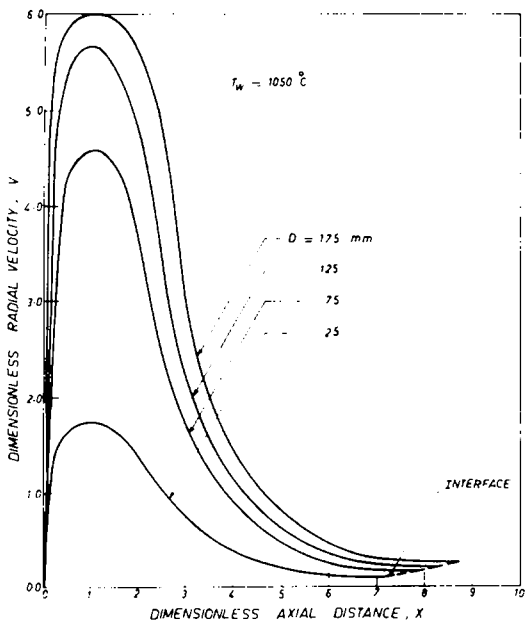

FIG. 5(b). Variation of radial velocity with depth, $T_w = 1050°C$.

The average heat flux and heat-transfer coefficient for any plate of radius R_0 is calculated by integrating equations (27), (28) using the trapezoidal rule [8].

3. RESULTS AND DISCUSSION

The boundary-layer equations (13) (15) are solved numerically for water at a range of wall temperatures of 450–1050°C and plate diameters up to 250 mm. Typical velocity and temperature profiles are shown on Figs. 4–7. The vapour film thickness distribution, and local and average heat-transfer coefficient and heat flux are shown on Figs. 8–12.

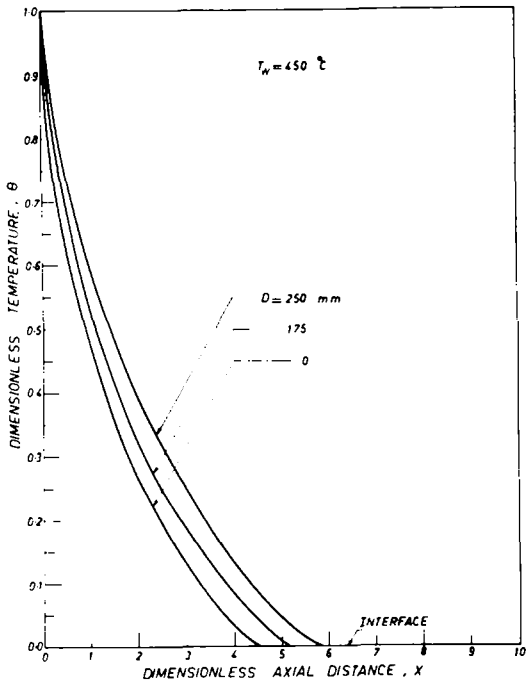

FIG. 6. Temperature distribution in the axial direction, $T_w = 450°C$.

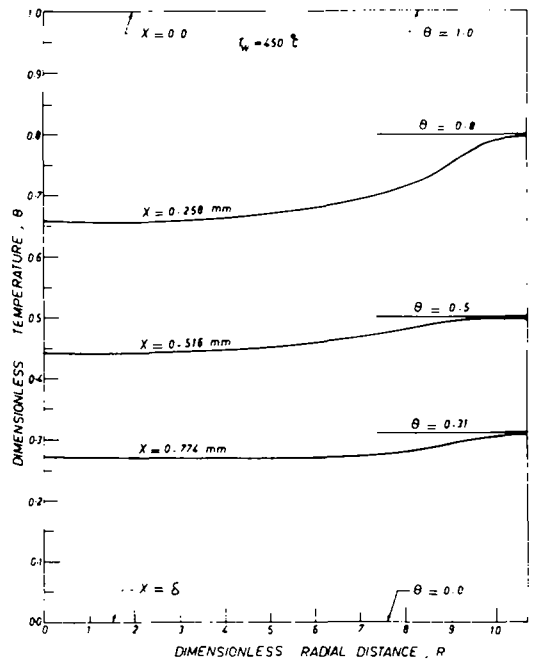

FIG. 7. Temperature distribution in the radial direction, $T_w = 450°C$.

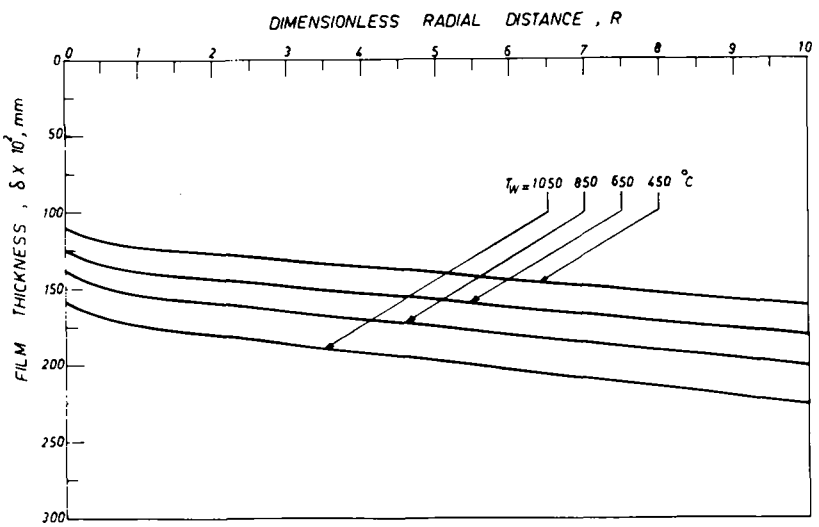

FIG. 8. Effect of surface temperature on film thickness distribution.

The effect of thermal radiation is not included in these results. This effect is considered negligible at $T_w = 450°C$. As the wall temperature is increased, radiation should be taken into consideration. It is expected therefore that the presented results may underestimate the value of heat-transfer rates at higher surface temperatures. It is conceivable, however, that the increased vapour generation rate, due to radiation, may be offset by the reduction in heat conduction due to increased film resistance.

At any depth X, the distribution of the vertical velocity component, Fig. 4, shows that U decreases with radial distance. Since U is directly related to the evaporation rate at the interface, it is to be expected that as the evaporation rate drops, the value of U decreases. It can be seen in Fig. 9 that the heat-transfer coefficient decreases with the radial distance, thus reducing the evaporation rate.

When Fig. 4(a) and 4(b) are compared U is seen to increase with wall superheat, due to the increase of heat flux, hence evaporation rate as seen in Fig. 12.

The radial velocity component V, Fig. 5(a, b) increases from zero at the wall to a maximum then drops to a low value at the interface. The velocity V increases with radial distance as the total vapour flow increases. The wall superheat has a similar effect on V due to increased vapour generation rate.

The temperature distribution in the axial direction,

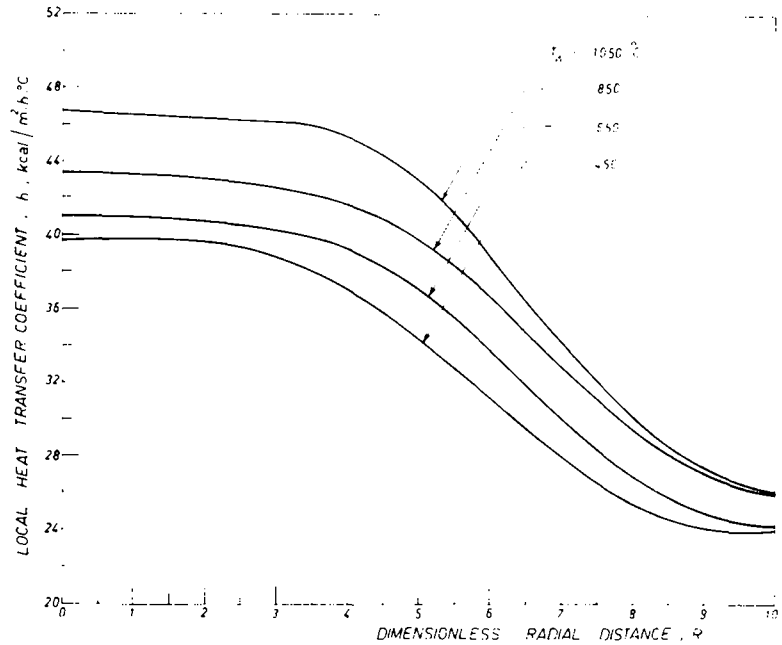

FIG. 9. Variation of local heat-transfer coefficient with radial distance.

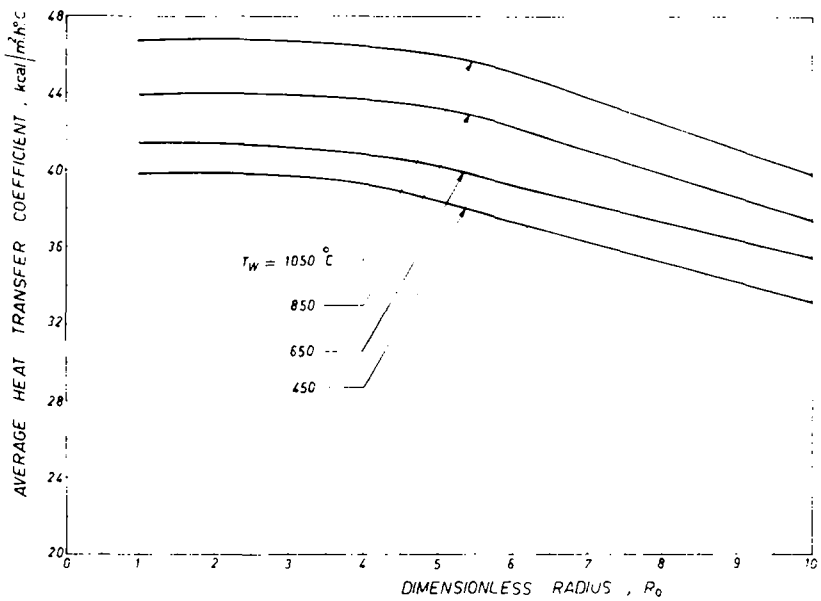

FIG. 10. Variation of average heat-transfer coefficient with plate radius.

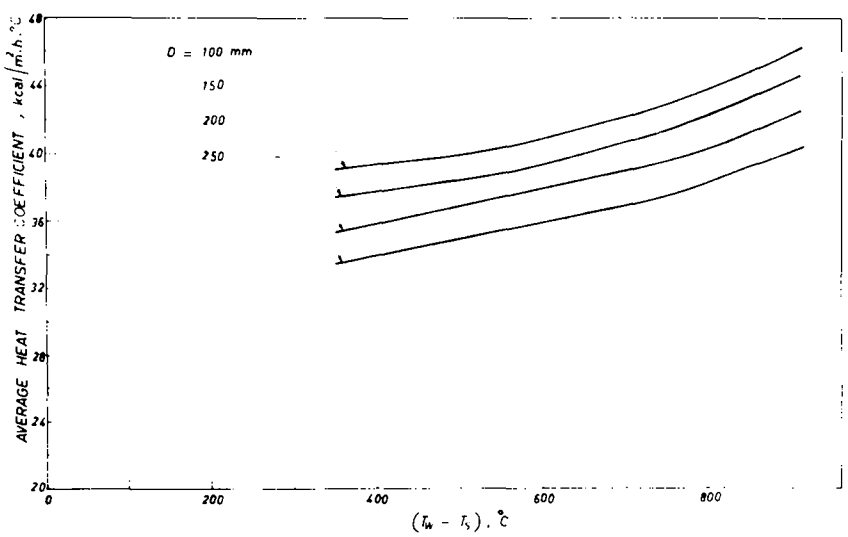

FIG. 11. Effect of wall superheat on average heat-transfer coefficient.

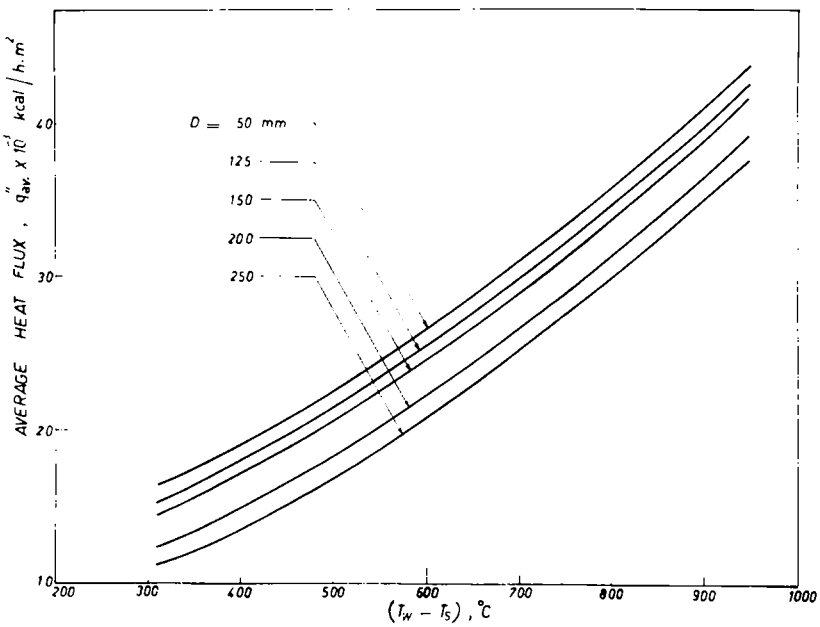

FIG. 12. Effect of wall superheat on average heat flux.

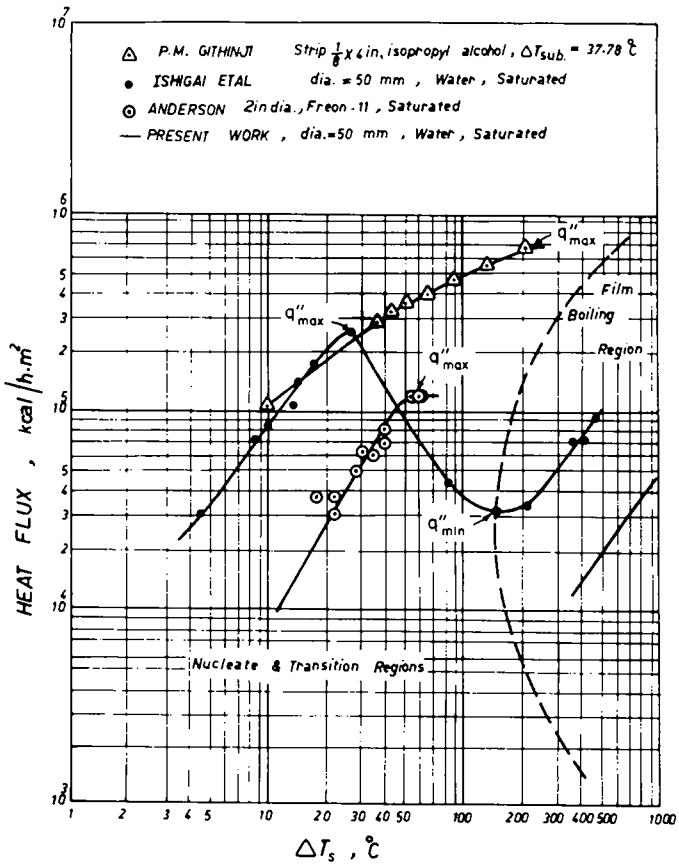

FIG. 13. Comparison with experimental data on boiling from downfacing plates.

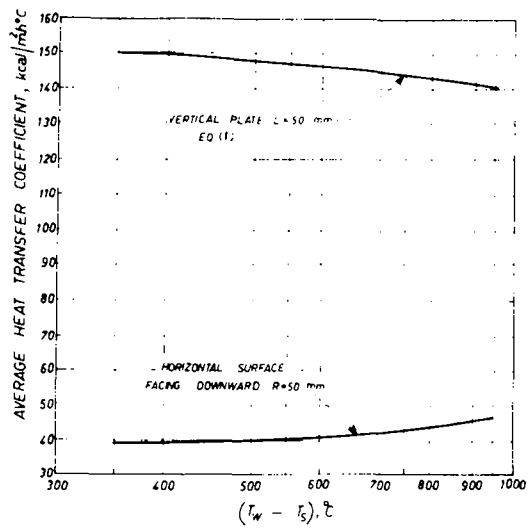

FIG. 14. Variation of average heat-transfer coefficient with plate dimension for vertical plates and horizontal plates facing downwards.

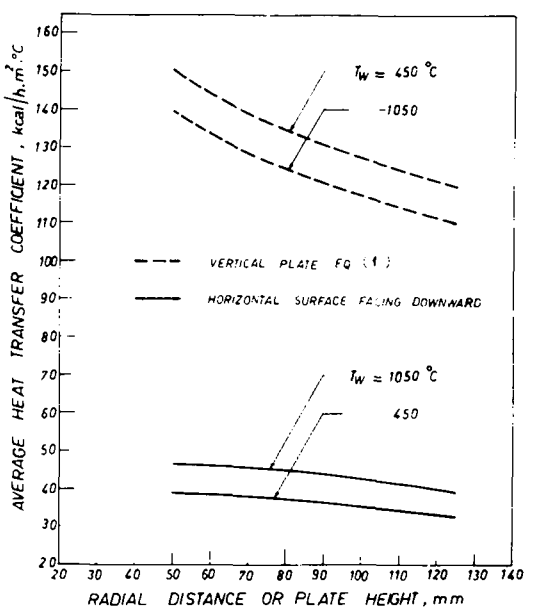

FIG. 15. Comparison of the effect of wall superheat on average heat-transfer coefficient for 50-mm. vertical plates and horizontal plates facing downwards.

Fig. 6, is nonlinear because of the convective effects. The dimensionless temperature decreases from its maximum value of 1.0 at the wall to its minimum value of zero at the interface. The temperature distribution in the radial direction is given on Fig. 7, at several fixed depths.

The film thickness distribution is shown on Fig. 8. The thickness increases rapidly near the plate axis then slows down further away. As the film thickness increases, resistance to heat transfer is increased. Consequently the rate of evaporation at the interface is reduced and the rate of thickness increase is diminished. This is reflected on the radial temperature distribution, Fig. 7, which tends to assume an asymptotic value at a given depth.

The temperature gradient at the wall is seen from Fig. 6, to decrease with plate radius, hence the heat flux and heat-transfer coefficients decrease in the radial direction as can be seen from Figs. 9–12. The typical film portions of the boiling curve for a heated plate facing downwards are given in Figs. 11 and 12.

Figure 13 shows the reported experimental data of boiling from down facing horizontal plates. Only those data of Ishigai *et al.* [4] contain some data points in the film boiling region. These are higher than our calculated results. One of the possible reasons is our neglect of radiation heat transfer. That does not seem, however, to account for the observed difference. The authors of [4] reported a strong dependence of their results on the end effects. They used an unheated ring on the plate periphery to avoid that effect.

This decreased the burnout heat flux appreciably. A doubling of the ratio of outside diameter of the unheated plate to that of the heated plate resulted in a decrease of burnout heat flux of more than 50%. In our analysis, end effects are neglected and this may well explain the lowered value of our results over those reported in [4].

4. CONCLUDING REMARKS

It is interesting to try to answer two important questions. (1) Does film boiling from vertical plates have any similarity to that from downward facing plates? (2) Are heat-transfer coefficients for both geometries comparable for small size plates?

There is a definite resemblance between the two geometries in film boiling. The vapour film grows gradually from the lower part (vertical), or central part (horizontal) of the plate until it reaches the edge, and is released upwards to the bulk liquid. The temperature profile, and the distribution of the velocity component parallel to the plate in both geometries behave similarly.

The distribution of the velocity component normal to the plate surface is different in either case. While U decreases monotonically from the interface to the plate wall in case of the vertical plate, it peaks inside the vapour film for the case of a downward facing plate. Gravity plays an important role in that respect.

Heat-transfer coefficients, however, are quite different. The results of Bromley's equation (1) are compared to the results of the present analysis for plates of similar dimensions immersed in saturated water, Fig. 14. It is clear that for the same wall superheat, average heat-transfer coefficients for vertical plates are several times higher than those for plates facing downwards. It can also be seen from Fig. 15 that whereas heat-transfer coefficients increase with wall superheat for plates facing downwards, they decrease slightly for vertical plates.

It may thus be concluded that velocity and temperature profiles in film boiling from plates facing downwards bear some similarity to those from the vertical plate, but the heat-transfer coefficients are quite different.

REFERENCES

1. L. A. Bromley, Heat transfer in stable film boiling, AEC-2295 (1948).
2. Y. P. Chang, Wave theory of heat transfer in film boiling, *J. Heat Transfer* **81**(1), 1 (1959).
3. L. A. Bromley, Heat transfer in stable film boiling, *Chem. Engng Prog.* **46**, 221 (1950).
4. S. I. Ishigai, K. Inoue, Z. Kiwaki and T. Inai, Heat transfer from a flat surface facing downward, Int. Ht. Tr. Conf., paper 26, 224 (1 September 1961).
5. P. M. Githinji and R. H. Sabersky, Some effects of the orientation of the heating surface in nucleate boiling, *J. Heat Transfer* **87**, 379 (November 1963).
6. R. P. Anderson and L. Bova, The role of downfacing burnout in post-accident heat removal, *Trans. Am. Nucl. Soc.* **14**, 294 (1971).
7. B. Carnahan, *Applied Numerical Methods*. John Wiley, New York (1960).
8. S. D. Conte, *Elementary Numerical Analysis*. McGraw-Hill, New York (1960).

TRANSFERT THERMIQUE AVEC EBULLITION STABLE EN FILM POUR UNE PLAQUE PLANE HORIZONTALE TOURNEE VERS LE BAS

Résumé—On présente une analyse de la convection naturelle, stable, laminaire pour une ébullition en film contre une plaque circulaire, isotherme, horizontale tournée vers le bas et submergée par un liquide saturé.

On utilise les techniques mathématiques de la théorie de la couche limite et on résout numériquement, par une méthode de différence explicite, les équations de continuité, de quantité de mouvement et d'énergie.

Des résultats sont obtenus pour l'eau saturée à la pression atmosphérique, des températures de paroi entre 450°C et 1050°C et pour des diamètres de plaque allant jusqu'à 250 mm.

WÄRMEÜBERGANG BEI STABILEM FILMSIEDEN AN DER UNTERSEITE EINER EBENEN, HORIZONTALEN PLATTE

Zusammenfassung—Es wird über eine Untersuchung des Wärmeübergangs bei stabilem, laminarem Filmsieden bei freier Konvektion an der Unterseite einer isothermen, ebenen, kreisförmigen, in gesättigte Flüssigkeit eingetauchten Platte berichtet. Es werden die mathematischen Methoden der Grenzschichttheorie angewandt; unter Verwendung einer expliziten Differenzentechnik werden die Kontinuitäts-, Impuls- und Energiegleichung für die Dampfphase numerisch gelöst. Für gesättigtes Wasser unter atmosphärem Druck werden Ergebnisse für Plattentemperaturen von 450°C bis 1050°C und Plattendurchmesser bis zu 250 mm angegeben.

ТЕПЛООБМЕН ПРИ ОБТЕКАНИИ ПЛОСКОЙ ГОРИЗОНТАЛЬНОЙ ПЛАСТИНЫ В УСЛОВИЯХ УСТОЙЧИВОГО ПЛЕНОЧНОГО КИПЕНИЯ

Аннотация — Анализируется процесс теплообмена от изотермической, горизонтально расположенной круглой пластины, погруженной в жидкость при ламинарной свободной конвекции и устойчивом пленочном кипении на поверхности. При анализе используется математическая модель теории пограничного слоя; с помощью явного разностного метода численно решены уравнения неразрывности, количества движения и сохранения энергии для паровой фазы. Получены результаты для насыщенной воды при атмосферном давлении, температуре пластины от 450 до 1050°C и диаметром пластины до 250 мм.